Kenneth R. Muske
Professor
Department of Chemical Engineering,
Villanova University,
Villanova, PA 19085

Hashem Ashrafiuon[1]
Director and Professor
e-mail: hashem.ashrafiuon@villanova.edu

Sergey Nersesov
Associate Professor

Mehdi Nikkhah[2]
Research Assistant

Department of Mechanical Engineering,
Center for Nonlinear Dynamics and Control,
Villanova University,
Villanova, PA 19085

Optimal Sliding Mode Cascade Control for Stabilization of Underactuated Nonlinear Systems

This paper presents an optimal sliding mode cascade control for stabilization of a class of underactuated nonlinear mechanical systems. A discrete-time, nonlinear model predictive control structure is used to optimally select and update the parameters of the sliding mode control surfaces at specified intervals in order to achieve a desired performance objective. The determination of these surface parameters is subject to constraints that arise from the stability conditions imposed by the sliding mode control law and the physical limits on the system such as input saturation. Nominal stability of the optimal cascade control structure is demonstrated and its robust performance is illustrated using an experimental rotary inverted pendulum system. [DOI: 10.1115/1.4005367]

1 Introduction

Model predictive control (MPC) has been widely applied to nonlinear systems as discussed in the extensive review article by Ref. [1]. MPC allows for optimal performance based on a specified objective, while satisfying all the constraints arising from stability and system's physical limitations. However, predictive control requires on-line optimization resulting in computation times that can limit its applicability in mechanical systems with fast dynamics. Recent progress in fast nonlinear MPC algorithms have begun to address this issue [2], however, the complexity involved in the algorithm development and numerical solution techniques still pose a challenge. The robustness of these controllers to numerical failure of the on-line optimization algorithms also remains a limitation.

MPC application to underactuated nonlinear mechanical systems with fast dynamics has been limited. Oh and Sun [3] developed an MPC for line-of-sight path generation and way-point tracking of underactuated surface vessels with input constraints where computational speed is not critical. Wen et al. [4] applied a nonlinear MPC to three-axis attitude control of fully actuated and underactuated spacecrafts where the control action at each time instance is determined based on the future predicted trajectory. Oliveira and Lages [5] applied nonlinear model based on the predictive control to develop a control input sequence that moves forward a brachiation robot on a horizontal line. Varga and Lantos [6] developed an MPC for underactuated nonlinear mechanical systems moving along a known reference path such as the inverted pendulum. However, they generalized the predictive control algorithm of linear time-invariant systems to linearized time variant systems rather than using a truly nonlinear controller. Jung and Wen [7] presented a nonlinear MPC for swing-up of a rotary inverted pendulum with iterative refinement and where the only objective is to reduce error. The experimental results show a lack of consistency and robustness in the balancing.

Sliding mode control (SMC) [8] is a robust stabilizing nonlinear control law that computes quickly and reliably, making it suitable for systems with fast dynamics. The dynamic performance of a sliding mode controller, however, is a complex function of the effort, surface, and system parameters. The control law is comprised of a reaching phase where the trajectory reaches the surface and a sliding phase where it slides to the origin. The main disadvantage of SMC is chattering around the surface during the sliding phase due to use of the discontinuous sign function, which is normally approximated by a continuous function. Another disadvantage of the controller is that it normally requires high gains particularly during its reaching phase. Hence, there have been some attempts to optimally redefine the sliding surfaces [9–13].

SMC has been widely used for underactuated mechanical systems. Bergerman and Xu [14] introduced variable structure controllers for robots by physically locking joints that are not being controlled using an iterative process. Lee et al. [15] developed specific set point sliding control laws for planar 2-link and 3-link robots under the influence of gravity. Su and Stepanenko [16] introduced a SMC for serial underactuated robots under the influence of gravity. Xu and Ozgüner [17] propose a sliding mode control law for a class of underactuated mechanical systems that can be represented in normal form and satisfy invertability conditions as discussed by Olfati-Saber [18]. They apply this method to flight control of a quad-rotor helicopter. Park et al. [19] and Martinez et al. [20] developed sliding mode controllers for two degrees-of-freedom (DOF) underactuated mechanical systems. The earlier method is based on decomposition of the system into two subsystems and was applied to simulate the inverted pendulum on the cart problem, while the later method used dry friction to essentially lock a joint (DOF) when positioning the other. Lee et al. [21] also developed an SMC by decomposing the underactuated mechanical system into subsystems and applied it to an overhead crane (pendulum on a cart) system. Sankaranarayanan and Mahindrakar [22] present a sliding mode control algorithm to stabilize a class of underactuated mechanical systems that are not linearly controllable and violate Brockett's necessary condition for smooth asymptotic stabilization of the equilibrium point [23]. Riachy et al. [24] propose a second order sliding mode control for underactuated systems that are applied to stabilization of an inverted pendulum. Santiesteban et al. [25] apply the same approach to swing-up control of the inverted pendulum. Ashrafiuon and Erwin [26] presented a sliding mode control for two different classes of mechanical systems based on the existence of isolated equilibrium and Brockett's necessary condition for smooth asymptotic stabilization and applied it to the inverted pendulum on a cart problem.

[1]Corresponding author.
[2]Currently a postdoctoral research fellow at Harvard-MIT Division of Health Sciences and Technology, Cambridge, MA 02139.

Contributed by the Dynamic Systems Division of ASME for publication in the Journal of Dynamic Systems, Measurement, and Control. Manuscript received July 23, 2010; final manuscript received September 6, 2011; published online January 12, 2012. Assoc. Editor: Nabil Chalhoub.

The approach was later applied to an experimental rotational/translational proof-mass actuator system by Avis et al. [27].

Model predictive and sliding mode control approaches have been previously combined to produce more effective controllers [28–30]. However, none seem suitable for underactuated nonlinear mechanical systems with fast dynamics. Zhou et al. [30] introduced a discrete-time nonlinear sliding mode model predictive controller where MPC is used to predesign the switching function and applied it to simulate a simple second order undamped system. Garcia-Gabin and Camacho [28] developed a predictive sliding mode controller for nonlinear nonminimum phase systems and demonstrated considerable improvements in terms of stability and robustness in a reactor system example compared with MPC. Perez et al. [29] introduced a predictive sliding mode controller to improve performance and robustness of nonlinear processes that can be represented as first order system plus a dead time.

In this work, a multirate cascade control structure is proposed that optimally adjusts the parameters of SMC developed in Ref. [26] using an MPC controller. By combining MPC and SMC in this fashion, it is possible to achieve near-optimal performance while also providing the computation time necessary for predictive control. A simple block diagram of the control structure is shown in Fig. 1. There are a number of advantages to the proposed approach. Stabilization of the nonlinear system can be maintained even when the predictive controller fails to obtain a numerical solution to the on-line optimization problem. This aspect of the approach is particularly attractive when the controlled target is an unstable equilibrium point of the system. Common performance objectives, such as minimum energy and minimum time, can easily be incorporated into the sliding mode control framework. By optimizing the specified performance objective under sliding mode control, undesirable state trajectories can be eliminated through the use of dynamic state constraints in the optimization problem. Constraints in this optimization can also include maximum and minimum saturation limits on the control actuators. The result is a nonlinear optimization problem similar to that posed in nonlinear predictive control. In this case, however, the decision variables are the surface parameters for the sliding mode controller as opposed to the future control trajectory.

The paper is constructed as follows. A brief discussion of the sliding mode controller for underactuated nonlinear systems with bounded disturbances begins the presentation. The proposed optimizing sliding mode control structure is presented and nominal stability is demonstrated. Minimum-time problems are then addressed. The paper closes with an experimental example based on the Quansar SRV-02 rotary inverted pendulum.

2 Sliding Mode Controller

Sliding mode control law is based on defining exponentially stable sliding surfaces as a function of the output errors [8]. It is constructed such that the nominal error trajectories reach these surfaces in finite time, referred to as the reaching phase, and then follow the sliding surfaces toward the origin, referred to as the sliding phase. The derivation and application of sliding mode control laws to fully actuated nonlinear mechanical systems is well documented in the literature. A detailed derivation can be found in the texts by Slotine and Li [31] and Khalil [32]. However, the SMC law for fully actuated systems cannot be applied to an underactuated system without modifications.

Consider an n DOF underactuated mechanical system with a generalized position vector, $q \in \mathbb{R}^n$, partitioned as $q = \left[q_a^{\mathrm{T}}, q_u^{\mathrm{T}}\right]^{\mathrm{T}}$, where $q_a \in \mathbb{R}^m$ is a vector of actuated coordinates and $q_u \in \mathbb{R}^{n-m}$ is a vector of unactuated coordinates. Then, the equations of motion for this system can be written as

$$\begin{bmatrix} M_{aa}(q) & M_{au}(q) \\ M_{au}^{\mathrm{T}}(q) & M_{uu}(q) \end{bmatrix} \begin{bmatrix} \ddot{q}_a \\ \ddot{q}_u \end{bmatrix} = \begin{bmatrix} f_a(q,\dot{q}) \\ f_u(q,\dot{q}) \end{bmatrix} + \begin{bmatrix} u \\ 0 \end{bmatrix} + \begin{bmatrix} g_a(q,\dot{q}) \\ g_u(q,\dot{q}) \end{bmatrix} \tag{1}$$

where $u \in \mathbb{R}^m$ is the control input, $f(q,\dot{q}) \triangleq [f_a^{\mathrm{T}}(q,\dot{q}), f_u^{\mathrm{T}}(q,\dot{q})]^{\mathrm{T}}$ is the vector of Coriolis, centrifugal, conservative, and nonconservative forces, and $g(q,\dot{q}) \triangleq [g_a^{\mathrm{T}}(q,\dot{q}), g_u^{\mathrm{T}}(q,\dot{q})]^{\mathrm{T}}$ represents the vector of bounded disturbances and uncertainties in the system. The positive definite inertia matrix is accordingly partitioned into positive definite matrices $M_{aa}: \mathbb{R}^n \to \mathbb{R}^{m\times m}$ and $M_{uu}: \mathbb{R}^n \to \mathbb{R}^{(n-m)\times(n-m)}$, and an off-diagonal matrix $M_{au}: \mathbb{R}^n \to \mathbb{R}^{m\times(n-m)}$. Note that since the inertia matrix is positive definite, it follows and can be easily verified that

$$M_{aa}(q) - M_{au}(q)M_{uu}^{-1}(q)M_{au}^{\mathrm{T}}(q) > 0 \tag{2}$$

It follows from Eq. (1) that

$$\ddot{q}_u = M_{uu}^{-1}(q)[-M_{au}^{\mathrm{T}}(q)\ddot{q}_a + f_u(q,\dot{q}) + g_u(q,\dot{q})] \tag{3}$$

and, consequently

$$\begin{aligned} \ddot{q}_a = (M_{aa}(q) - M_{au}(q)M_{uu}^{-1}(q)M_{au}^{\mathrm{T}}(q))^{-1}[f_a(q,\dot{q}) + g_a(q,\dot{q}) \\ - M_{au}(q)M_{uu}^{-1}(q)(f_u(q,\dot{q}) + g_u(q,\dot{q})) + u] \end{aligned} \tag{4}$$

Next, using partial feedback linearization, the controller is given by

$$\begin{aligned} u = (M_{aa}(q) - M_{au}(q)M_{uu}^{-1}(q)M_{au}^{\mathrm{T}}(q))v - f_a(q,\dot{q}) \\ + M_{au}(q)M_{uu}^{-1}(q)f_u(q,\dot{q}) \end{aligned} \tag{5}$$

where $v \in \mathbb{R}^m$ is the new controller and Eqs. (3) and (4) can be rewritten as

$$\ddot{q}_a = v + \tilde{g}_a(q,\dot{q}) \tag{6}$$

$$\ddot{q}_u = M_{uu}^{-1}(q)f_u(q,\dot{q}) - M_{uu}^{-1}(q)M_{au}^{\mathrm{T}}(q)v + \tilde{g}_u(q,\dot{q}) \tag{7}$$

and the new uncertainty vectors are given by

$$\begin{aligned} \tilde{g}_a(q,\dot{q}) \triangleq (M_{aa}(q) - M_{au}(q)M_{uu}^{-1}(q)M_{au}^{\mathrm{T}}(q))^{-1} \\ \times [g_a(q,\dot{q}) - M_{au}(q)M_{uu}^{-1}(q)g_u(q,\dot{q})] \end{aligned} \tag{8}$$

$$\tilde{g}_u(q,\dot{q}) \triangleq M_{uu}^{-1}(q)[g_u(q,\dot{q}) - M_{au}^{\mathrm{T}}(q)\tilde{g}_a(q,\dot{q})] \tag{9}$$

Note that in this work, we assume a zero state target such that the position and velocity vectors $(q,\dot{q})$ represent the tracking error for the mechanical systems.

Next, consider a vector function $s \triangleq [s_1, \ldots, s_m]^{\mathrm{T}}: \mathbb{R}^n \times \mathbb{R}^n \to \mathbb{R}^m$ given by

$$\begin{aligned} s(q,\dot{q}) &= \alpha_a\dot{q}_a + \lambda_a q_a + \alpha_u\dot{q}_u + \lambda_u q_u \\ &= \alpha_a\dot{q}_a + \alpha_u\dot{q}_u + s_r(q) \end{aligned} \tag{10}$$

where $s \triangleq [s_1, \ldots, s_m]^{\mathrm{T}}: \mathbb{R}^n \times \mathbb{R}^n \to \mathbb{R}^m$, $s_r(q) \triangleq \lambda_a q_a + \lambda_u q_u$, and $\alpha_a \in \mathbb{R}^{m\times m}$, $\lambda_a \in \mathbb{R}^{m\times m}$, $\alpha_u \in \mathbb{R}^{m\times(n-m)}$, $\lambda_u \in \mathbb{R}^{m\times(n-m)}$ are the matrices of surface parameters such that $\alpha_a \in \mathbb{R}^{m\times m}$, $\lambda_a \in \mathbb{R}^{m\times m}$ are invertible and $\left(\alpha_a - \alpha_u M_{uu}^{-1}(q)M_{au}^{\mathrm{T}}(q)\right)^{-1}$ exists for all $q \in \mathcal{M} \subseteq \mathbb{R}^n$. We define the sliding surface as the null space of $s(\cdot,\cdot)$, that is

$$\mathcal{S} = \{(q,\dot{q}) \in \mathbb{R}^n \times \mathbb{R}^n : s(q,\dot{q}) = 0\} \tag{11}$$

As in standard SMC theory, the control law v is calculated by setting $\dot{s}(q,\dot{q}) = 0$ for the nominal system and adding a signum function to address uncertainties. Hence, using Eqs. (6) and (7)

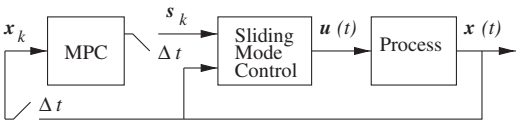

Fig. 1 Cascade controller block diagram

$$v = -(\alpha_a - \alpha_u M_{uu}^{-1}(q) M_{au}^{T}(q))^{-1} [\alpha_u M_{uu}^{-1}(q) f_u(q,\dot{q}) + \dot{s}_r(q) + K(q,\dot{q}) \text{sign}(s(q,\dot{q}))] \quad (12)$$

where $\text{sign}(s(q,\dot{q})) \triangleq [\text{sign}(s_1(q,\dot{q})), \ldots, \text{sign}(s_m(q,\dot{q}))]^T$, $K(q,\dot{q}) \triangleq \text{diag}[k_1(q,\dot{q}), \ldots, k_m(q,\dot{q})]$,

$$k_i(q,\dot{q}) = \eta_i + \|\text{row}_i^T(\alpha_a)\|_1 \|\tilde{g}_a(q,\dot{q})\|_\infty + \|\text{row}_i^T(\alpha_u)\|_1 \|\tilde{g}_u(q,\dot{q})\|_\infty, \quad i = 1, \ldots, m \quad (13)$$

$\eta_i > 0$, and $\text{row}_i(\cdot)$ is the ith row of a matrix.

Remark 1. Note that a less conservative than Eq. (13) but constant estimate of the control gain k_i, $i = 1,\ldots,m$, can be chosen to be

$$k_i = \eta_i + \|\text{row}_i^T(\alpha_a)\|_1 \sup_{(q,\dot{q}) \in \mathbb{R}^n \times \mathbb{R}^n} \|\tilde{g}_a(q,\dot{q})\|_\infty + \|\text{row}_i^T(\alpha_u)\|_1 \sup_{(q,\dot{q}) \in \mathbb{R}^n \times \mathbb{R}^n} \|\tilde{g}_u(q,\dot{q})\|_\infty \quad (14)$$

provided that the above supremums are finite.

Remark 2. Sliding mode control will always result in chattering around the surfaces due to the signum function in Eq. (12). In practice, the discontinuous sign function is often approximated by a continuous function, such as the hyperbolic tangent, or by a linear saturation function inside a boundary layer around each surface $s(q,\dot{q}) = 0$ to avoid chattering. A similar approximation may be applied to the underactuated sliding mode control law presented here.

Next, we show that with the feedback control law (12), the trajectories of the closed-loop system (6), (7) converge to the sliding surface (11) in finite time. To see this, consider a Lyapunov function given by

$$V(q,\dot{q}) = \frac{1}{2} s^T(q,\dot{q}) s(q,\dot{q}) \quad (15)$$

The Lyapunov time derivative, $\dot{V}(q,\dot{q}) = s^T(q,\dot{q})\dot{s}(q,\dot{q})$, is derived using the derivative of the surfaces defined in Eq. (11) and by substituting from Eqs. (6), (7), and (12)

$$\dot{V}(q,\dot{q}) \le -\sum_{i=1}^{m} \left[k_i(q,\dot{q}) - \|\text{row}_i^T(\alpha_a)\|_1 \|\tilde{g}_a(q,\dot{q})\|_\infty - \|\text{row}_i^T(\alpha_u)\|_1 \|\tilde{g}_u(q,\dot{q})\|_\infty\right] |s_i(q,\dot{q})|$$

Substituting from Eq. (13) into the previous equation and noting that $\|s\|_2 = \sqrt{2}(V(q,\dot{q}))^{\frac{1}{2}}$, the finite time reaching condition can be determined as

$$\dot{V}(q,\dot{q}) = -\sum_{i=1}^{m} \eta_i |s_i(q,\dot{q})| \le -\sqrt{2} \min_{i=1,\ldots,m} \{\eta_i\} (V(q,\dot{q}))^{\frac{1}{2}}, \quad (q,\dot{q}) \in \mathcal{M} \times \mathbb{R}^n \quad (16)$$

It was shown in Ref. [33] that condition (16) guarantees that the closed-loop system trajectories converge to the sliding surface (11) in finite time and remain on this surface, while the value of $\min_i = 1, \ldots, m\{\eta_i\}$ determines the rate of convergence. Furthermore, while on the sliding surface, the closed-loop dynamics are given by the following reduced-order system:

$$0 = \alpha_a \dot{q}_a + \lambda_a q_a + \alpha_u \dot{q}_u + \lambda_u q_u \quad (17)$$

$$\ddot{q}_u = \tilde{M}_1(q) f_u(q,\dot{q}) + \tilde{M}_2(q)(\lambda_a \dot{q}_a + \lambda_u \dot{q}_u) + \tilde{g}_u(q,\dot{q}) \quad (18)$$

where the second equation is derived by substituting for the control law in Eq. (12) into Eq. (7) and letting $s(q,\dot{q}) = 0$ and

$$\tilde{M}_1(q) \triangleq M_{uu}^{-1}(q) + M_{uu}^{-1}(q) M_{au}^T(q) \times (\alpha_a - \alpha_u M_{uu}^{-1}(q) M_{au}^T(q))^{-1} \alpha_u M_{uu}^{-1}(q) \quad (19)$$

$$\tilde{M}_2(q) \triangleq M_{uu}^{-1}(q) M_{au}^T(q) (\alpha_a - \alpha_u M_{uu}^{-1}(q) M_{au}^T(q))^{-1} \quad (20)$$

The stability of the reduced order closed-loop dynamics represented by Eqs. (17) and (18) can be established based on the existence of isolated equilibrium points.

Remark 3. Isolated equilibrium points can be determined for a given system if they are constrained to a manifold of dimension less than or equal to m. This constraint is only possible in the presence of potential energy where conservative forces are only a function of position. Otherwise, there are infinitely many equilibrium points. Systems with infinite number of equilibrium points are not time-invariant continuous feedback stabilizable [23]. For these systems, only marginal stability exists in cases where momentum is conserved and a discontinuous control law is necessary. Further discussion on this topic can be found in Ref. [26].

In this work, systems with isolated equilibrium points are considered where the system is linearly controllable around these points as shown in Ref. [34].

Remark 4. Stabilization of a nonlinear system under sliding mode control can be established through the use of a system specific Lyapunov function as presented in Ref. [35] and adopted in Appendix for the experimental system considered in this work.

3 Model Predictive Control

The primary controller in the proposed cascade control structure is a discrete-time, nonlinear model predictive controller that re-optimizes the sliding mode controller linear surface parameters at each sample period. In addition to improving performance, the control structure ensures asymptotic stability in presence of actuator input and other system constraints.

3.1 Infinite Horizon Problems. An infinite horizon performance objective following the Lagrange cost function in optimal control [36] is considered

$$\min_p J_k = \int_{k\Delta t}^{\infty} \Phi(x,u) dt \quad (21)$$

where $J_k \in \mathbb{R}$ is the objective function value at sample time k, Δt is the discrete sample period, $\Phi : (\mathbb{R}^n \times \mathbb{R}^n) \to \mathbb{R}$ is the performance penalty function, $p \in \mathbb{R}^{4m}$ is the vector of linear surface parameters, $x = [q^T, \dot{q}^T]^T \in \mathbb{R}^{2n}$ is the state vector of the system, and $u \in \mathbb{R}^m$ is the control. The objective function is minimized over the surface parameters p subject to the following constraints

$$\dot{x} = h(x,u) \quad (22)$$

$$u = c(x,p) \quad (23)$$

$$p \in \mathcal{P}, \quad x \in \mathcal{X}, \quad u \in \mathcal{U} \quad (24)$$

$$w(x,u) \le 0 \quad (25)$$

in which $h : (\mathbb{R}^{2n} \times \mathbb{R}^m) \to \mathbb{R}^{2n}$ is the dynamic equality constraint arising from the system equations, $c : (\mathbb{R}^{2n} \times \mathbb{R}^{4m}) \to \mathbb{R}^m$ is the sliding mode control law, $\mathcal{P} \in \mathbb{R}^{4m}$ is the constraint space for the surface parameters p, $\mathcal{X} \in \mathbb{R}^{2n}$ is the constraint space for the state, $\mathcal{U} \in \mathbb{R}^m$ is the constraint space for the control, and $w : (\mathbb{R}^{2n} \times \mathbb{R}^m) \to \mathbb{R}^r$ represents r general inequality constraints on the states and control. We note that $\mathcal{P}$ represents the inequality constraints on the surface parameters that arise from the surface stability criteria for underactuated systems [26] and $\mathcal{X}$, $\mathcal{U}$ represent inequality constraints on the state and control. Incorporating the sliding mode control law into the performance penalty function $\Phi(\cdot)$ in Eq. (21)

$$\Psi(x,p) = \Phi(x, c(x,p)) \quad (26)$$

It is assumed that $\phi(\cdot)$ is a positive function with the following properties:

$$c_1\|x\|^2 \leq \phi(x,s) \leq c_2\|x\|^2 \tag{27}$$

$$\Psi(x,p) = 0 \quad \text{iff} \quad x = 0 \tag{28}$$

for all $p \in \mathcal{P}$ and $t \geq 0$ where c_1 and c_2 are strictly positive real constants.

3.2 Nominal Stability. Nominal stability of the closed-loop cascade control structure shown in Fig. 1 with the infinite horizon Lagrange cost function in Eq. (21) subject to the constraints and restrictions in Eqs. (22)–(28) is demonstrated in this section. We assume no disturbances and begin with some preliminary results concerning feasibility and boundedness. Note that, however, bounded disturbances are accounted for in the SMC.

Lemma 1. *Feasibility of the constrained optimization problem in Eqs. (21)–(25) at sample time $k=k^*$ for the nominal system with no disturbances implies feasibility at every sample time $k>k^*$.*

Proof. Feasibility implies a set of nominally stable surface parameters that satisfy the constraints in Eqs. (22)–(25) for all $t \geq k^*\Delta t$. Therefore, this set must also be feasible for all future sample times for the disturbance-free nominal system. Since at least one feasible set of surface parameters exist, the constrained optimization problem is feasible for all $k>k^*$.

Lemma 2. *Feasibility of the constrained optimization problem in Eqs. (21)–(25) at sample period k implies that the objective J_k is bounded.*

Proof. Feasibility implies the existence of an exponentially stable sliding mode controller that reaches the surface in finite time. Exponential stability of the sliding mode controller implies that the integral $\int_{k\Delta t}^{\infty}\|x\|^2 dt$ is bounded, which then implies that the objective J_k is bounded from the inequality in Eq. (27).

Lemma 3. *The sequence of open-loop optimal objective function values for the feasible constrained optimization problem in Eqs. (21)–(25), $\{\tilde{J}_k\}$, converges to some non-negative value $\tilde{J}_\infty$ for the nominal system.*

Proof. Let $\tilde{J}_k$ denotes the optimal value of the objective in Eq. (21) at time k, and $\hat{J}_{k+1}$ denotes the value of the objective at time $k+1$ using the same surface parameters as time k. From Lemmas 1 and 2, $\hat{J}_{k+1}$ exists and is bounded. The following relationship then holds:

$$\tilde{J}_k = \hat{J}_{k+1} + \hat{\mathcal{J}}_{k+1}, \quad \hat{\mathcal{J}}_{k+1} = \int_{k\Delta t}^{(k+1)\Delta t} \Psi(x,p)d\tau$$

Optimization at time $k+1$ results in an objective value that can be no greater than $\hat{J}_{k+1}$ which implies $\tilde{J}_{k+1} \leq \hat{J}_{k+1}$ and the following inequality:

$$\tilde{J}_k \geq \tilde{J}_{k+1} + \hat{\mathcal{J}}_{k+1}$$

Since $\Psi(\cdot)$ is a positive function, $\tilde{J}_k$ and $\hat{\mathcal{J}}_k$ are both positive functions, and the sequence $\{\tilde{J}_k\}$ is nonincreasing and bounded below by zero. Therefore, it converges to a non-negative value.

Theorem 1. *For the closed-loop cascade control structure with the infinite horizon objective function in Eq. (21) subject to the constraints in Eqs. (22)–(25) and no disturbances, the origin is nominally asymptotically stable for all feasible initial states.*

Proof. Nominal asymptotic stability of the origin follows from stability of the origin and convergence. Feasibility of the constrained optimization problem in Eqs. (21)–(25) for the initial state implies convergence of the sequence $\{\tilde{J}_k\}$ from Lemma 3. Convergence of the sequence $\{\tilde{J}_k\}$ implies that the sequence $\{\hat{\mathcal{J}}_k\}$ converges to zero as follows. Since the sequence $\{\tilde{J}_k\}$ is nonincreasing and converges to $\tilde{J}_\infty$, it follows that $\hat{\mathcal{J}}_{k+1} \leq \tilde{J}_k - \tilde{J}_\infty$ for all $k>0$. It also follows that for every $\varepsilon>0$, there exists a $k^*(\varepsilon)$ such that $\tilde{J}_k - \tilde{J}_\infty \leq \varepsilon$ for all $k>k^*(\varepsilon)$. Therefore, $\hat{\mathcal{J}}_k \leq \varepsilon$ for all $k>k^*(\varepsilon)+1$. Since $\Psi(\cdot)$ is a positive function, the mean value theorem ensures that the function $\Psi(\cdot)$ converges to zero if its time integral over one sample period Δt converges to zero. From Eq. (28), the state must then also converge to zero.

Remark 5. The infinite horizon may be approximated by finite horizon using a finite prediction horizon, while maintaining the stability as suggested in Ref. [37]. However, a large finite horizon could result in large computation times. Thus, a terminal zero state penalty, as presented in Sec. 3.3, is used for a finite horizon approximation.

3.3 Minimum-Time Problems. Nominal stability for the cascade control structure presented in Sec. 3.2 is a consequence of the infinite receding horizon employed for the objective in Eq. (21). A second common method for ensuring nominal stability for model predictive control is through the use of a terminal state constraint [1]. This formulation is applicable to minimum-time problems where the time interval is minimized subject to achieving some desired final value of the state. The objective becomes

$$\min_p J_k = \int_{k\Delta t}^{t_{f_k}+k\Delta t} 1dt = t_{f_k} \tag{29}$$

minimized over the surface parameters p subject to a terminal state constraint at the final time t_{f_k}

$$h(x(t_{f_k})) = 0 \tag{30}$$

and the constraints in Eqs. (22)–(24). The dependence of the final time on the sample period is denoted by the subscript k. The terminal state constraint in Eq. (30) may be specified such that the ℓ^2-norm of the state vector is equal to zero. However, since sliding mode control is exponentially stable and does not reach the origin exactly in finite time, the terminal state constraint is defined in the following inequality form:

$$\|x\|_2 = [x^T x]^{1/2} \leq \nu \tag{31}$$

where $0<\nu<<1$

Lemma 4. *Feasibility of the constrained optimization problem in Eqs. (29), (30), (22)–(24) at sample time $k=0$ for the nominal system with no disturbances implies feasibility at every sample time $k>0$.*

Proof. Feasibility at sample time $k>0$ follows in the same manner as Lemma 1. Satisfaction of the terminal constraint in Eq. (30) implies that is t_{f_k} bounded for all $k \geq 0$.

Theorem 2. *For the closed-loop cascade control structure with the minimum-time objective function in Eq. (29) subject to the constraints in Eqs. (22)–(24), (30) and no disturbances, the final state satisfies the terminal constraint in time $t<t_{f_o}$ for all feasible initial states.*

Proof. Initial feasibility of the minimum-time optimization problem implies that it is feasible for all $k>0$ and that t_{f_o} is bounded from Lemma 4. Using the argument presented in the proof of Lemma 3, optimization guarantees that

$$t_{f_{k+1}} \leq t_{f_k} - \Delta t$$

which implies that

$$t_{f_k} \leq t_{f_o} - \Delta t$$

by induction. Since t_{f_o} is bounded, there exists a k^* such that $t_{f_{k^*}}$ is minimum. Therefore, the sequence $\{t_{f_k}\}$ is bounded above by $t_{f_o} - \Delta t$ for all $k<k^*$, which proves the theorem.

Remark 6. The sliding mode control derived in Eq. (12), guarantees closed-loop stability during each progressing Δt sample period for all bound uncertainties and disturbances, which are presented in Eq. (1) as $g_a(q,\dot{q})$ and $g_u(q,\dot{q})$. These uncertainties/disturbances are only accounted for in terms of their bounds in the

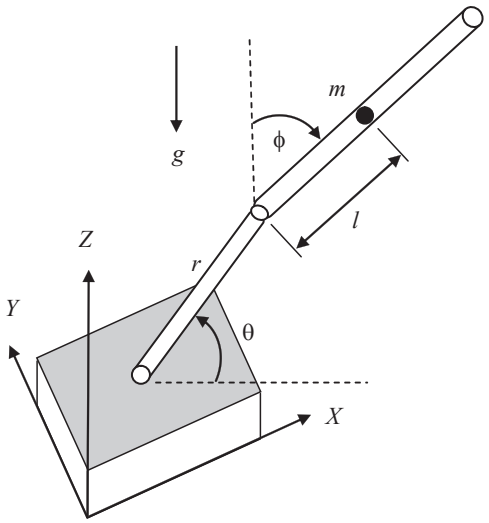

Fig. 2 The rotary inverted pendulum

control gains presented in Eqs. (13) and (14). Thus, the optimal parameter selection will be unaffected if the bounds for uncertainties and disturbances remain the same and there are no time varying structural changes. However, the cascade structure is open-loop and predictive only. Thus, optimality of the solution cannot be guaranteed if there are any unpredicted changes in the structure and magnitude of disturbances or uncertainties.

4 Experimental Example

The model-based cascade sliding mode control structure is applied to the Quansar SRV-02 rotary inverted pendulum experimental system in this example. A schematic of the rotary inverted pendulum is shown in Fig. 2. The system has two degrees-of-freedom, the pendulum arm angle, ϕ, and the rotating arm angle, θ. The single actuator is a dc motor and gearbox connected to the rotating arm. The equations of motion for the system are [38]

$$c\ddot{\phi} - b\cos\phi\ddot{\theta} = d\sin\phi + c\sin\phi\cos\phi\dot{\theta}^2 \tag{32}$$

$$-b\cos\phi\ddot{\phi} + (a + c\sin^2\phi)\ddot{\theta} = -b\sin\phi\dot{\phi}^2 - 2c\sin\phi\cos\phi\dot{\phi}\dot{\theta} - b_e\dot{\theta} + a_e u \tag{33}$$

where the pendulum arm angle ϕ and the rotating arm angle θ are the outputs, the dc motor voltage u is the input, r_o is the length of the rotating arm, l is one half the length of the pendulum arm, d_e is the equivalent system damping coefficient, and a_e is the motor actuator torque constant, $c = \frac{4}{3}m_o l^2$, $b = m_o l r_o$, $a = I_e + m_o r_o^2$, I_e is the equivalent inertia of the rotating arm, motor, and gearbox, m_o is the pendulum arm mass, and g is the gravitational constant. The parameter values for the experimental system are as follows: $l = 0.1675$ m, $r_o = 0.215$ m, $m = 0.125$ kg, $I_e = 0.0036$ kg m^2, $d_e = 0.073$ N m s/rad, and $a_e = 0.1285$ Nm/V.

The sliding mode control law is derived by defining the scalar sliding surface

$$s = \alpha_a\dot{\theta} + \lambda_a\theta + \alpha_u\dot{\phi} + \lambda_u\phi \tag{34}$$

and using Eqs. (5) and (12). The closed-loop dynamics and exponential stability of the system specific sliding mode controller is presented in Appendix. However, simpler conditions for stability of the sliding surface, which can be incorporated into constraints in Eq. (24) may be derived as

$$\alpha_a, \lambda_a < 0 \quad \alpha_u, \lambda_u > 0 \tag{35}$$

$$\frac{\lambda_a}{\alpha_a} < \frac{\lambda_u}{\alpha_u} \tag{36}$$

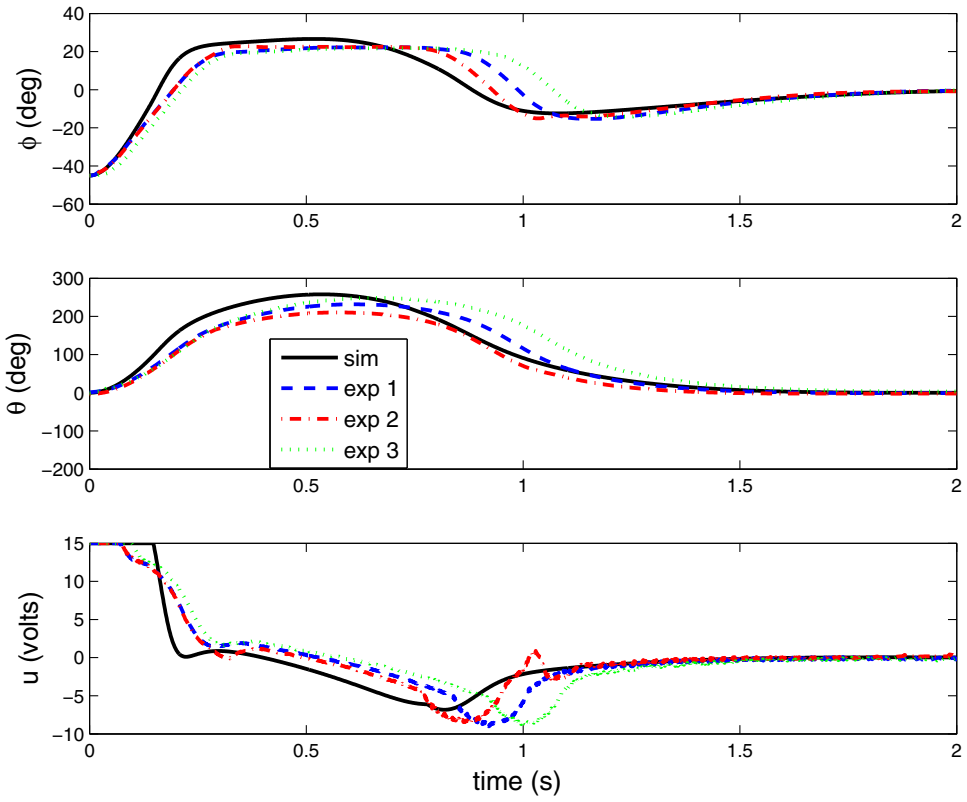

Fig. 3 Comparison of simulation and experimental results; (top) pendulum arm angle (middle), rotating arm angle (bottom), control input voltage

Table 1 Surface parameters and objective function values for the minimum energy problem

Parameter	Base case	Initial optimal	MPC cascade
α_u	5	1.94	1.94, 2.18, 2.5, 2.46
λ_u	10	11.14	11.14, 13.37, 15.27, 15.25,…
λ_a	−0.5	−0.248	−0.248, −0.1, −0.107, −0.1,…
Total cost	44.7	17.6	15.7

$$c\alpha_a + b\cos\theta\alpha_u > 0 \tag{37}$$

The sliding mode control law u is updated by the discrete model predictive controller at a control interval of $\Delta t = 0.1$ s. There are four surface parameters that can be selected and updated to minimize a given performance objective in this example. However, due to normalization, only three are independent. The last three surface parameters are selected as the decision variables for the optimization resulting in $p = [\lambda_a, \alpha_u, \lambda_u]^T$ The first surface parameter is selected as $\alpha_a = -1$ since surface normalization will result in only three independent surface parameters. A gain of $\eta = 20$ is used for the effort parameter in the reaching condition. The maximum motor voltage input position constraint is

$$|u| \leq v_{\max} \tag{38}$$

where $v_{\max} = 15$ V. Also, a linear saturation function is used to approximate the signum function in order to avoid chattering

$$\text{sat}(s/\varepsilon_s) = \begin{cases} s/\varepsilon_s & \text{if} |s| \leq \varepsilon_s \\ \text{sign}(s) & \text{if} |s| > \varepsilon_s \end{cases} \tag{39}$$

where the surface boundary layer thickness is selected as $\varepsilon_s = 0.1$. The minimum-time control problem in this example has discontinuous gradients requiring the implementation of a nongradient based optimization procedure in this example. A similar result was observed in previous work with the inverted pendulum on a cart system in Ref. [13].

The performance of the MPC cascade control structure in this work is compared to that of a base case feasible surface design and an initial optimal surface design. A single optimization of the surface parameters is carried out at time $t = 0$ for the initial optimal surface. Both minimum energy and minimum-time performance objectives are considered. In these examples, it is desired to move the system to the origin from an initial pendulum arm angle $|\phi(0)|$ between 40 deg and 45 deg. Note that, a swing-up control algorithm such as the one presented in Ref. [7] may be used to swing the pendulum arm to the initial angle.

In order to demonstrate model fidelity, the simulated and actual experimental state trajectories and control input of the sliding mode controller for the rotary inverted pendulum system are compared in Fig. 3. The surface parameters selected for this demonstration are those derived for the "initial optimal" minimum-time values presented in Table 2. The results are shown for three repeating experiments where very good agreement with the simulation results can be observed. The small differences in the experiments are mainly due to motor friction.

4.1 Minimum Energy Controller. The minimum energy control objective at each sample period is

$$\min_p J_k = \int_{t=k\Delta t}^{\infty} u^2 dt \tag{40}$$

subject to the model equality constraint in Eqs. (32) and (33), surface parameter constraints in Eqs. (35)–(37), and the control saturation bound in Eq. (38). We have also used the terminal state

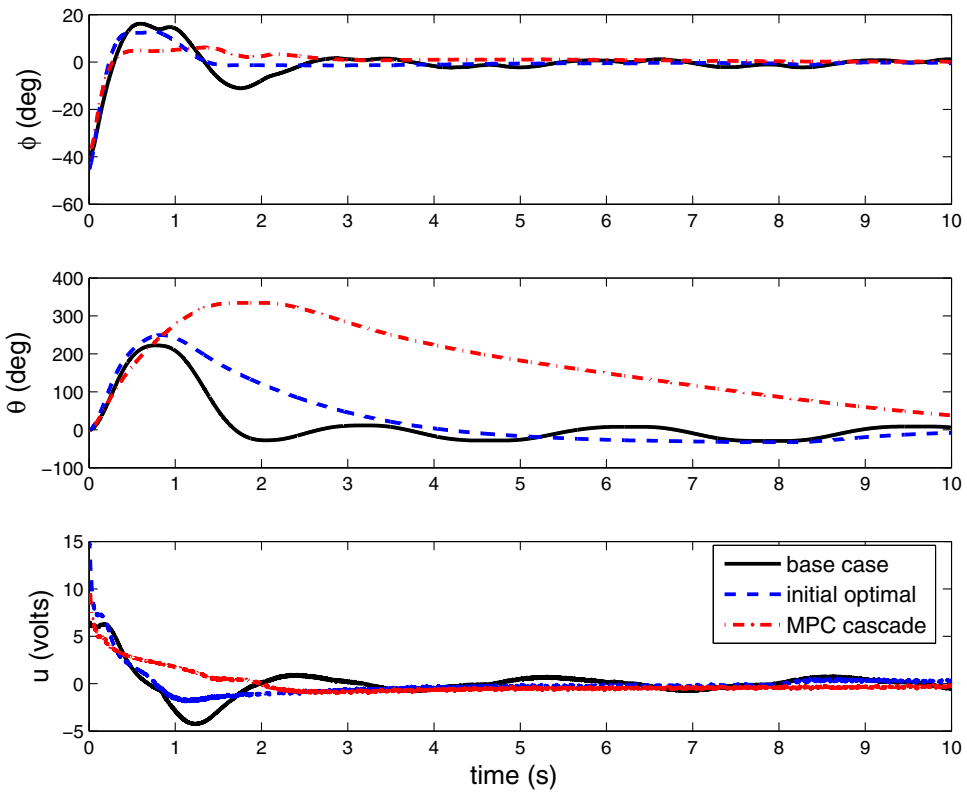

Fig. 4 Comparison of experimental initial feasible design (base case), one-time optimization (initial optimal), and MPC cascade control (MPC cascade) for the minimum-energy problem; (top) pendulum arm angle, (middle) rotating arm angle, (bottom) control input voltage

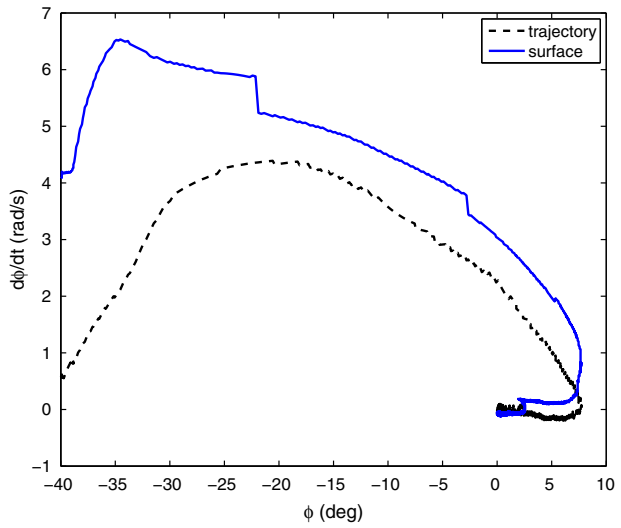

Fig. 5 Experimental reaching and sliding phases with the surface changes for the minimum-energy MPC cascade controller

constraint in Eq. (31) with $\nu = 0.01$ to approximate the infinite horizon problem with a finite horizon one.

Table 1 presents a comparison of the surface parameters and total cost for the base case surface parameters (base case), the initial surface optimization (initial optimal), and the model predictive cascade control in this work (cascade MPC). The base case parameters were selected based on the stability conditions presented in Eqs. (35)–(37) to yield a feasible solution for optimization. The initial set of surface parameters for the cascade controller is the same as the initial one-time optimization solution. Only the first four sets of surface parameters are presented for the cascade control because the surface parameters essentially converged to these values after four sample periods. The total cost is computed from the control trajectory determined by the sliding mode controllers in each case. As shown in Table 1, initial one-time optimization of the surface parameters results in a significant cost reduction of almost 61%. The cascade controller results in an additional 11% reduction in cost compared to the initial optimal surface. Note that, the finite time horizon implemented based on Eq. (31) with $\nu = 0.01$ varies during the optimization but never exceeds 17 s.

Table 2 Surface parameters and objective function values for the minimum-time problem

Parameter	Base case	Initial optimal	MPC cascade
α_u	5	1.96	1.96, 1.5, 1.49, 1.49
λ_u	10	12.1	12.1, 9.69, 9.66, 9.66
λ_a	−0.5	−1.59	−1.59, −2.36, −2.4, −2.4
Total cost	16.2	2.8	2.0

The surface parameters listed in Table 1 were experimentally implemented for real-time sliding mode control of the rotary inverted pendulum. Figure 4 compares the controller performance for the base case feasible surface, the initial one-time optimal surface, and the MPC cascade control optimal surfaces. It is clear that the parameters derived from initial optimization and MPC cascade control improve the performance if the controller both in terms pendulum arm stabilization and control effort with the MPC cascade control outperforming the one-time optimal controller. However, the rotating arm stabilizes at a much slower rate for the MPC cascade controller compared to the other two (approximately 14 s) since there is no penalty associated with its tracking error. Essentially, the optimal solution sacrifices the rotating arm position, which is not crucial to the pendulum stabilization in

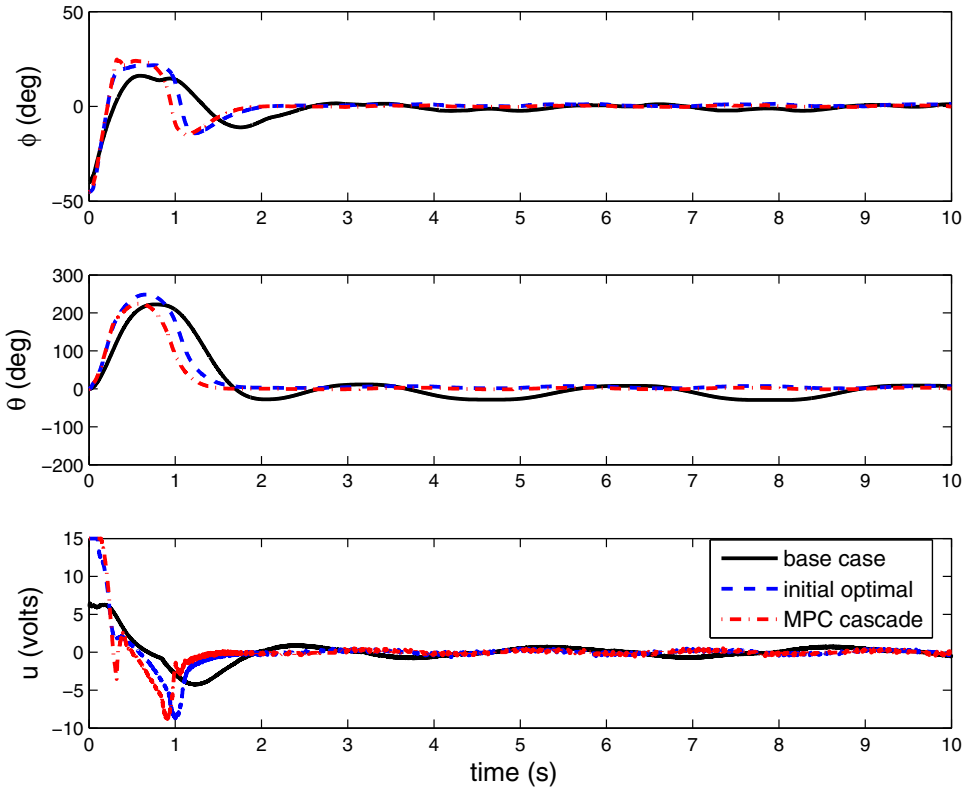

Fig. 6 Comparison of experimental initial feasible design (base case), one-time optimization (initial optimal), and MPC cascade control (MPC cascade) for the minimum-time problem; (top) pendulum arm angle (middle), rotating arm angle (bottom), control input voltage

order to minimize controller effort. The phase plot of the experimental pendulum arm angle trajectory versus the surface changes in the MPC cascade control is shown in Fig. 5. It can be seen from the experiment that the surface changes, as observed in the discontinuities in the surface plot, result in apparent jumps toward the trajectory hence reducing the total effort for the MPC cascade controller. Note that, the surface as displayed in the pendulum arm angle phase plot is not a linear line due to its dependency on θ and $\dot{\theta}$.

4.2 Minimum-Time Controller. The minimum-time control objective at each sample period is

$$\min_{p} J_k = t_{f_k} \tag{41}$$

subject to the model equality constraint in Eqs. (32) and (33), surface parameter constraints in Eqs. (35)–(37), the control saturation bound in Eq. (38), and the terminal constraint on the ℓ^2-norm of the system state presented in Eq. (31) with $\nu = 0.01$ where the state vector is defined as $x = [\theta, \phi, \dot{\theta}, \dot{\phi}]^{\mathrm{T}}$. Table 2 presents a comparison of the surface parameters and total time for the base case surface parameters (base case), the initial one-time optimization (initial optimal), and the model predictive cascade control (cascade MPC). Only the first four sets of surface parameters are presented for the cascade control because the surface parameters in this example also essentially converged to these values after four sample periods. The total time is computed from the state trajectory in each case. Initial one-time optimization of the surface parameters results in a significant cost reduction of almost 83%. While the cascade controller provides an additional 29% reduction in cost compared to the initial optimal surface.

The surface parameters listed in Table 2 were experimentally implemented for real-time SMC of the rotary inverted pendulum. Figure 6 compares the controller performance for the base case feasible surface, the initial one-time optimal surface, and the MPC cascade control optimal surfaces. It can be seen that the parameters derived from initial one-time optimization and MPC cascade control improve the stabilization time for both pendulum and rotating arm angles with the MPC cascade control outperforming the one-time optimal controller. However, larger efforts with larger variations are required for both the initial optimal and the MPC cascade controllers.

5 Conclusions

A nominally stabilizing, nonlinear, model-based sliding mode cascade control structure is demonstrated in this work where disturbances are accounted for in the context of the sliding mode control. Nonlinear model predictive control is used as the primary loop in this control structure to update the surface parameters of the secondary sliding mode controller in order to achieve a specified performance objective. As indicated by the rotary inverted pendulum experimental results, significant improvement in the sliding mode controller performance can be achieved by optimally updating the sliding surface using this approach for both minimum energy and minimum-time control objectives.

Acknowledgment

Partial support for this work from the Office of Naval Research under Grant No. N00014-09-1-1195 and the use of the experimental facilities of the Center for Nonlinear Dynamics and Control (CENDAC) at Villanova University are gratefully acknowledged.

Appendix

In this Appendix, we show that the controlled system, while on the sliding surface, is locally exponentially stable. To see this, consider the sliding surface equation

$$0 = \alpha_\theta \dot{\theta}(t) + \lambda_\theta \theta(t) + \alpha_\phi \dot{\phi}(t) + \lambda_\phi \phi(t), \quad t \geq t^* \tag{A1}$$

along with the closed-loop system dynamics given by

$$\begin{aligned}(\alpha_\theta c + \alpha_\phi b \cos\phi(t))\ddot{\phi}(t) = &- b\lambda_\phi \dot{\phi}(t)\cos\phi(t) + \alpha_\theta d \sin\phi(t) \\ &- \lambda_\theta b \dot{\theta}(t)\cos\phi(t) \\ &+ \alpha_\theta m l^2 \dot{\theta}^2(t)\sin\phi(t)\cos\phi(t), \\ &\phi(t^*) = \phi^*, \quad \dot{\phi}(t^*) = \dot{\phi}^*\end{aligned} \tag{A2}$$

$$\begin{aligned}(\alpha_\theta c + \alpha_\phi b \cos\phi(t))\ddot{\theta}(t) = &- c\lambda_\phi \dot{\phi}(t) - \alpha_\phi d \sin\phi(t) \\ &- c\lambda_\theta \dot{\theta}(t) - \alpha_\phi m l^2 \dot{\theta}^2(t)\sin\phi(t)\cos\phi(t), \\ &\theta(t^*) = \theta^*, \quad \dot{\theta}(t^*) = \dot{\theta}^*\end{aligned} \tag{A3}$$

where $t^* \in [0, \infty)$ is the instant when the closed-loop system state reaches the sliding surface (A1) and $\phi^*, \theta^*, \dot{\phi}^*, \dot{\theta}^* \in \mathbb{R}$ are corresponding system angular positions and velocities at $t = t^*$. Next, introduce state vector $x = [x_1, x_2, x_3, x_4]^{\mathrm{T}} \triangleq [\theta, \phi, \dot{\theta}, \dot{\phi}]^{\mathrm{T}}$ so that the system dynamics (A2) and (A3) can be rewritten as

$$\dot{x}_1(t) = x_3(t), \quad x_1(t^*) = \theta^*, \quad t \geq t^* \tag{A4}$$

$$\dot{x}_2(t) = x_4(t), \quad x_2(t^*) = \phi^* \tag{A5}$$

$$\dot{x}_3(t) = \frac{-c\lambda_\theta\left[x_3(t) + \frac{\lambda_\phi}{\lambda_\theta}x_4(t)\right] - \alpha_\phi d \sin x_2(t) - \alpha_\phi m l^2 x_3^2(t)\sin x_2(t)\cos x_2(t)}{\alpha_\theta c + \alpha_\phi b \cos x_2(t)} \quad x_3(t^*) = \dot{\theta}^* \tag{A6}$$

$$\dot{x}_4(t) = \frac{-\lambda_\theta b \cos x_2(t)\left[x_3(t) + \frac{\lambda_\phi}{\lambda_\theta}x_4(t)\right] + \alpha_\theta d \sin x_2(t) + \alpha_\theta m l^2 x_3^2(t)\sin x_2(t)\cos x_2(t)}{\alpha_\theta c + \alpha_\phi b \cos x_2(t)} \quad x_4(t^*) = \dot{\phi}^* \tag{A7}$$

and the sliding surface Eq. (A1) becomes

$$0 = \alpha_\theta x_3(t) + \lambda_\theta x_1(t) + \alpha_\phi x_4(t) + \lambda_\phi x_2(t), \quad t \geq t^* \tag{A8}$$

Note that the closed-loop system (A4)–(A7), while on the sliding surface (A8), can be characterized by a reduced third-order model. To obtain the reduced-order system, define an auxiliary variable

$$z \triangleq x_1 + \frac{\lambda_\phi}{\lambda_\theta}x_2 \tag{A9}$$

and note that the sliding surface Eq. (A8) becomes

$$\dot{z}(t) = -\frac{\lambda_\theta}{\alpha_\theta}z(t) - \alpha x_4(t), \quad t \geq t^* \tag{A10}$$

where $\alpha \triangleq \frac{\alpha_\phi}{\alpha_\theta} - \frac{\lambda_\phi}{\lambda_\theta}$. Since $\dot{x}_2(t) = x_4(t)$ and $\dot{z}(t) = x_3(t) + \frac{\lambda_\phi}{\lambda_\theta} x_4(t)$, it follows that, while on the sliding surface, the closed-loop system dynamics are given by

$$\ddot{x}_2(t) = \frac{-\lambda_\theta b \cos x_2(t)\dot{z}(t) + \alpha_\theta d \sin x_2(t)\left[1 + \frac{ml^2}{d} x_3^2(t)\cos x_2(t)\right]}{\alpha_\theta c + \alpha_\phi b \cos x_2(t)}, \quad t \geq t^* \tag{A11}$$

$$\dot{z}(t) = -\frac{\lambda_\theta}{\alpha_\phi} z(t) - \alpha \dot{x}_2(t) \tag{A12}$$

Next, introduce state variables $y_1 \triangleq x_2$, $y_2 \triangleq \dot{x}_2$, $y_3 \triangleq z$, and a constant

$$\varepsilon \triangleq -\frac{\alpha_\theta c}{\alpha_\phi b} \in (0, 1) \tag{A13}$$

so that the closed-loop system dynamics (A11) and (A12) can be rewritten in the state-space form as follows:

$$\dot{y}_1(t) = y_2(t) \tag{A14}$$

$$\dot{y}_2(t) = \frac{\frac{\lambda_\theta \alpha}{\alpha_\phi} y_2(t) + \frac{\lambda_\theta^2}{\alpha_\phi \alpha_\theta} y_3(t)}{1 - \frac{\varepsilon}{\cos y_1(t)}} + \frac{\alpha_\theta d \tan y_1(t)}{\alpha_\phi b\left(1 - \frac{\varepsilon}{\cos y_1(t)}\right)} - \frac{\varepsilon m l^2 \left(\left(\alpha + \frac{\lambda_\phi}{\lambda_\theta}\right) y_2(t) + \frac{\lambda_\theta}{\alpha_\phi} y_3(t)\right)^2 \sin y_1(t)}{c\left(1 - \frac{\varepsilon}{\cos y_1(t)}\right)} \tag{A15}$$

$$\dot{y}_3(t) = -\alpha y_2(t) - \frac{\lambda_\theta}{\alpha_\theta} y_3(t) \tag{A16}$$

In order to avoid singularity in Eq. (A15), we consider $y_1 \equiv \phi \in I \triangleq \{y_1 \in \mathbb{R} : -\arccos(\varepsilon) < y_1 < \arccos(\varepsilon)\}$ and define $\mathcal{D} \triangleq \{y \in \mathbb{R}^3 : y_1 \in I\}$, where $y \triangleq [y_1, y_2, y_3]^{\mathrm{T}}$. In this case, $1 - \frac{\varepsilon}{\cos y_1} > 0$, $y_1 \in I$. Next, to show exponential stability of the system (A14)–(A16), consider a Lyapunov function candidate

$$V(y) = \frac{1}{2} y^{\mathrm{T}} P y - \beta \ln \frac{\cos y_1 - \varepsilon}{1 - \varepsilon}, \quad y \in \mathcal{D} \tag{A17}$$

where $\beta > 0$, $P \in \mathbb{R}^{3\times 3}$ is such that $P > 0$, and

$$P = \begin{bmatrix} p_{11} & p_{12} & p_{13} \\ p_{12} & p_{22} & 0 \\ p_{13} & 0 & p_{33} \end{bmatrix} \tag{A18}$$

Note that $V(0) = 0$ and $V(y) > 0$, $y \in \mathcal{D}$, $y \neq 0$. Next, using the fact that $y_1 \tan y_1 > y_1^2$, $y_1 \in I$, it can be shown that, with

$$\beta = -\frac{p_{22}\alpha_\theta d}{\alpha_\phi b} > 0 \tag{A19}$$

and $|p_{12}| > |p_{22}|$, the Lyapunov derivative along trajectories of Eqs. (A14)–(A16) satisfies

$$\dot{V}(y) \leq -\frac{1}{2} y^{\mathrm{T}} R(y_1) y, \quad y \in \mathcal{D} \tag{A20}$$

where

$$R(y_1) = \begin{bmatrix} r_{11}(y_1) & r_{12}(y_1) & r_{13}(y_1) \\ r_{12}(y_1) & r_{22}(y_1) & r_{23}(y_1) \\ r_{13}(y_1) & r_{23}(y_1) & r_{33}(y_1) \end{bmatrix} \tag{A21}$$

where

$$\begin{aligned} r_{11}(y_1) &= -\frac{2p_{12}\alpha_\theta d}{\alpha_\phi b\left(1 - \frac{\varepsilon}{\cos y_1}\right)} \\ r_{12}(y_1) &= -p_{11} + \alpha p_{13} - \frac{p_{12}\alpha\lambda_\theta}{\alpha_\phi\left(1 - \frac{\varepsilon}{\cos y_1}\right)} \\ r_{13}(y_1) &= \frac{p_{13}\lambda_\theta}{\alpha_\theta} - \frac{p_{12}\lambda_\theta^2}{\alpha_\phi\alpha_\theta\left(1 - \frac{\varepsilon}{\cos y_1}\right)} \\ r_{22}(y_1) &= -2\left(p_{12} + \frac{p_{22}\alpha\lambda_\theta}{\alpha_\phi\left(1 - \frac{\varepsilon}{\cos y_1}\right)}\right) \\ r_{23}(y_1) &= -p_{13} + \alpha p_{33} - \frac{p_{22}\lambda_\theta^2}{\alpha_\phi\alpha_\theta\left(1 - \frac{\varepsilon}{\cos y_1}\right)} \\ r_{33}(y_1) &= 2\frac{p_{33}\lambda_\theta}{\alpha_\theta} \end{aligned} \tag{A22}$$

Next, we show that if $R(y_1) > 0$, $y_1 \in \tilde{I} \subseteq I$, then the closed-loop system (A14)–(A16) is locally exponentially stable. Assume $R(y_1) > 0$, $y_1 \in \tilde{I}$, and note that in this case

$$0 \leq \inf_{y_1 \in \tilde{I}} (\lambda_{\min}(R(y_1)))I_3 \leq R(y_1), \quad y_1 \in \tilde{I} \tag{A23}$$

where $\lambda_{\min}(R(y_1))$ is the minimal eigenvalue of $R(y_1)$ for some $y_1 \in \tilde{I}$ and $I_3 \in \mathbb{R}^{3\times 3}$ is the identity matrix. Furthermore, it follows from the Taylor series expansion around $y_1 = 0$ on the interval $y_1 \in \tilde{I}$ that, for every $\varepsilon > 0$ and $\beta > 0$, there exists sufficiently large $\gamma > 0$ such that

$$-\beta \ln \frac{\cos y_1 - \varepsilon}{1 - \varepsilon} \leq \frac{1}{2}\gamma y_1^2, \quad y_1 \in \tilde{I} \tag{A24}$$

In this case

$$\begin{aligned} V(y) &= \frac{1}{2} y^{\mathrm{T}} P y - \beta \ln \frac{\cos y_1 - \varepsilon}{1 - \varepsilon} \\ &\leq \frac{1}{2} y^{\mathrm{T}} P y + \frac{1}{2}\gamma y_1^2 \\ &= \frac{1}{2} y^{\mathrm{T}} \tilde{P} y, \quad y \in \tilde{\mathcal{D}} \end{aligned} \tag{A25}$$

where $\tilde{\mathcal{D}} \triangleq \{y \in \mathbb{R}^3 : y_1 \in \tilde{I}\}$ and

$$\tilde{P} \triangleq \begin{bmatrix} p_{11} + \gamma & p_{12} & p_{13} \\ p_{12} & p_{22} & 0 \\ p_{13} & 0 & p_{33} \end{bmatrix} \tag{A26}$$

Clearly, $\tilde{P} > 0$ since $P > 0$ and $\gamma > 0$. Thus, it follows from Eqs. (A23) and (A25) that

$$\begin{aligned} \dot{V} &\leq -\frac{1}{2} y^{\mathrm{T}} R(y_1) y \\ &\leq -\frac{1}{2} \inf_{y_1 \in \tilde{I}} (\lambda_{\min}(R(y_1))) y^{\mathrm{T}} y \\ &\leq -\frac{\inf_{y_1 \in \tilde{I}} (\lambda_{\min}(R(y_1)))}{\lambda_{\max}(\tilde{P})} V(y) \\ &= -\sigma V(y), \quad y \in \tilde{\mathcal{D}} \end{aligned} \tag{A27}$$

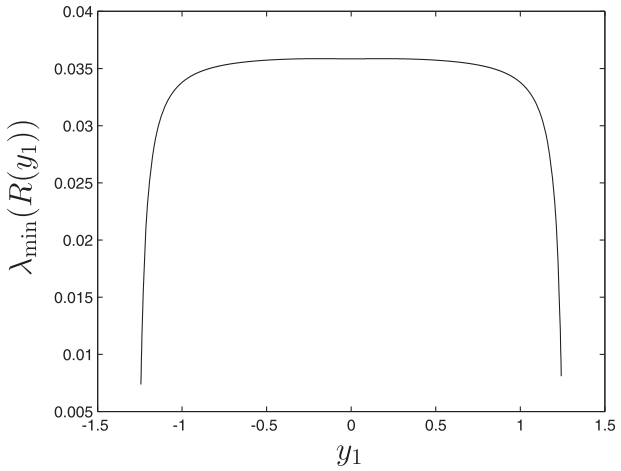

Fig. 7 Base case

where $\sigma \triangleq \frac{\inf_{y_1 \in \tilde{I}}(\lambda_{\min}(R(y_1)))}{\lambda_{\max}(\tilde{P})}$. Thus, if $\sigma > 0$, then Eqs. (A14)–(A16) are locally exponentially stable with the domain of attraction given by $\tilde{\mathcal{D}}$. Hence, the closed-loop system (A4)–(A7), while on the sliding surface (A8), is locally exponentially stable.

Next, for several cases of the sliding surface parameters, we show that the closed-loop system (A14)–(A16) is locally exponentially stable. We use numerical procedure involving linear matrix inequalities to obtain $P \in \mathbb{R}^{3\times3}$ in Eq. (A18) and $R(\cdot) \in \mathbb{R}^{3\times3}$ in Eq. (A21) such that $P > 0$ and $R(y_1) > 0$, $y_1 \in \tilde{I}$. The following system parameters in their corresponding units are used below, that is, $b = 0.0033$, $c = 0.0047$, and $d = 0.2054$.

(1) Base case. $\alpha_\theta = -1$, $\lambda_\theta = -0.5$, $\alpha_\phi = 5$, $\lambda_\phi = 10$. In this case, $\varepsilon = 0.2834$ and we choose $p_{11} = 50$, $p_{12} = 10$, $p_{13} = 1$, $p_{22} = 5$, and $p_{33} = 0.04$ so that $P > 0$. Here, $\beta = 62.2121$ and $\tilde{I} = \{y_1 \in \mathbb{R} : -\arccos(\varepsilon) + 004 \le y_1 \le \arccos(\varepsilon) - 004\} = [-1.24, 124]$. The plot of $\lambda_{\min}(R(y_1))$ versus $y_1 \in \tilde{I}$ is shown in Fig. 7. It can be seen from the plot that $\inf_{y_1 \in \tilde{I}}(\lambda_{\min}(R(y_1))) > 0$, and hence, Eq. (A27) is satisfied with $\sigma > 0$, which implies local exponential stability of Eqs. (A14)–(A16).

(2) Initial one-time optimization-minimum energy. $\alpha_\theta = -1$, $\lambda_\theta = -0.248$, $\alpha_\phi = 1.94$, $\lambda_\phi = 11.14$. In this case, $\varepsilon = 0.7304$, and we choose $p_{11} = 100$, $p_{12} = 10$, $p_{13} = 1$, $p_{22} = 2$, and $p_{33} = 0.03$ so that $P > 0$. Here, $\beta = 64.1362$ and $\tilde{I} = \{y_1 \in \mathbb{R} : -\arccos(\varepsilon) + 002 \le y_1 \le \arccos(\varepsilon) - 002\} = [-0.73, 073]$. The plot of $\lambda_{\min}(R(y_1))$ versus $y_1 \in \tilde{I}$ is shown in Fig. 8. It can be seen from the plot that $\inf_{y_1 \in \tilde{I}}(\lambda_{\min}(R(y_1))) > 0$, and hence, Eq. (A27) is satisfied with $\sigma > 0$, which implies local exponential stability of Eqs. (A14)–(A16).

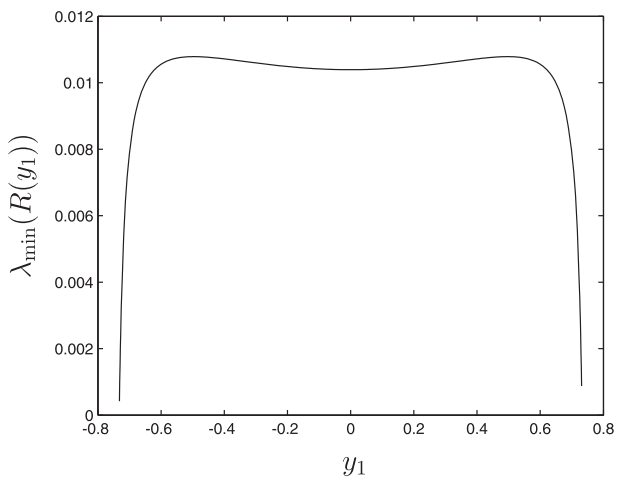

Fig. 8 Initial one-time optimization-minimum energy

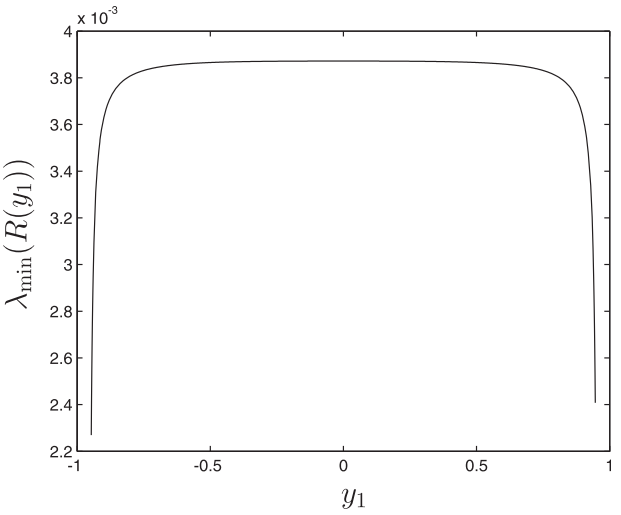

Fig. 9 MPC cascade controller-minimum energy

(3) MPC cascade controller-minimum energy. $\alpha_\theta = -1$, $\lambda_\theta = -0.1$, $\alpha_\phi = 2.46$, $\lambda_\phi = 15.25$. In this case, $\varepsilon = 0.4065$, and we choose $p_{11} = 1000$, $p_{12} = 70$, $p_{13} = 3$, $p_{22} = 10$, and $p_{33} = 0.02$ so that $P > 0$. Here, $\beta = 253.014$ and $\tilde{I} = \{y_1 \in \mathbb{R} : -\arccos(\varepsilon) + 001 \le y_1 \le \arccos(\varepsilon) - 001\} = [-0.95, 095]$. The plot of $\lambda_{\min}(R(y_1))$ versus $y_1 \in \tilde{I}$ is shown in Fig. 9. It can be seen from the plot that $\inf_{y_1 \in \tilde{I}}(\lambda_{\min}(R(y_1))) > 0$, and hence, Eq. (A27) is satisfied with $\sigma > 0$, which implies local exponential stability of Eqs. (A14)–(A16).

(4) Initial one-time optimization-minimum time. $\alpha_\theta = -1$, $\lambda_\theta = -1.59$, $\alpha_\phi = 1.96$, $\lambda_\phi = 12.1$. In this case, $\varepsilon = 0.723$, and we choose $p_{11} = 100$, $p_{12} = 10$, $p_{13} = 7$, $p_{22} = 2$, and $p_{33} = 1$ so that $P > 0$. Here, $\beta = 63.511$ and $\tilde{I} = \{y_1 \in \mathbb{R} : -\arccos(\varepsilon) + 024 \le y_1 \le \arccos(\varepsilon) - 024\} = [-0.52, 052]$. The plot of $\lambda_{\min}(R(y_1))$ versus $y_1 \in \tilde{I}$ is shown in Fig. 10. It can be seen from the plot that $\inf_{y_1 \in \tilde{I}}(\lambda_{\min}(R(y_1))) > 0$, and hence, Eq. (A27) is satisfied with $\sigma > 0$, which implies local exponential stability of Eqs. (A14)–(A16).

(5) MPC cascade controller-minimum time. $\alpha_\theta = -1$, $\lambda_\theta = -2.4$, $\alpha_\phi = 1.49$, $\lambda_\phi = 9.66$. In this case, $\varepsilon = 0.95$, and we choose $p_{11} = 40$, $p_{12} = 6$, $p_{13} = 10$, $p_{22} = 1$, and

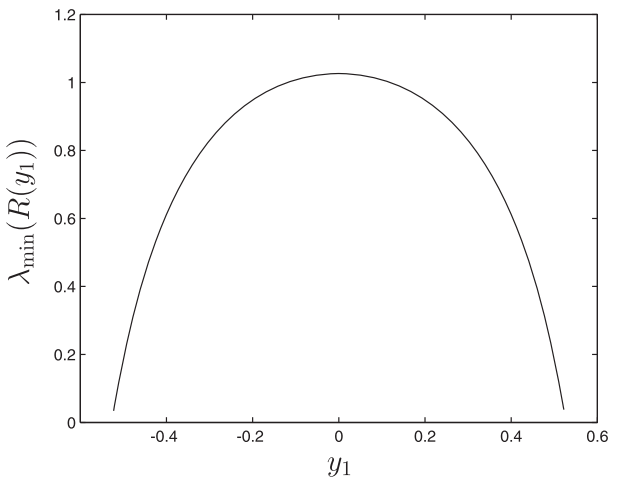

Fig. 10 Initial one-time optimization-minimum time

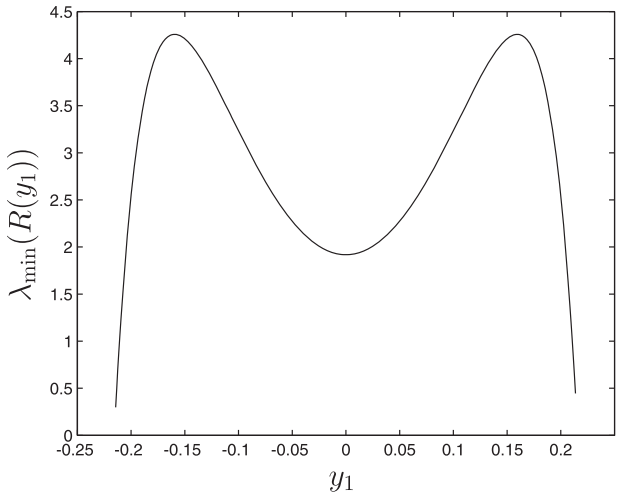

Fig. 11 MPC cascade controller-minimum time

$p_{33} = 40$ so that $P > 0$. Here, $\beta = 41.773$ and $\tilde{I} = \{y_1 \in \mathbb{R} : -\arccos(\varepsilon) + 01 \leq y_1 \leq \arccos(\varepsilon) - 01\} = [-0.22, 022]$. The plot of $\lambda_{\min}(R(y_1))$ versus $y_1 \in \tilde{I}$ is shown in Fig. 11. It can be seen from the plot that $\inf_{y_1 \in \tilde{I}}(\lambda_{\min}(R(y_1))) > 0$, and hence, Eq. (A27) is satisfied with $\sigma > 0$, which implies local exponential stability of Eqs. (A14)–(A16).

References

[1] Mayne, D. Q., Rawlings, J. B., Rao, C. V., and Skokart, P. O., 2000, "Constrained Model Predictive Control: Stability and Optimality," Automatica, **36**, pp. 789–814.

[2] Magni, L., and Raimondo, D. M., eds., F. A., 2009, *Nonlinear Model Predictive Control: Toward New Challenging Applications* (Lecture Notes in Control and Information Sciences 384), Springer-Verlag, Berlin/Heidelberg.

[3] Oh, S.-R., and Sun, J., 2010, "Path Following of Underactuated Marine Surface Vessels Using Line-of-Sight Based Model Predictive Control," Ocean Eng., **37**(2–3), pp. 289–295.

[4] Wen, J., Seereeram, S., and Bayard, D., 1997, "Nonlinear Predictive Control Applied to Spacecraft Attitude Control," *Proceedings of the 1997 American Control Conference (Cat. No.97CH36041)*, Vol. 3, pp. 1899–1903.

[5] de Oliveira, V., and Lages, W., 2007, "MPC Applied to Motion Control of an Underactuated Brachiation Robot," 2006 IEEE Conference on Emerging Technologies and Factory Automation (IEEE Cat. No.06TH8897).

[6] Varga, A., and Lantos, B., 2005, "Model Based Predictive Control of Underactuated Nonlinear Mechatronical Systems," Period. Polytech., Electr. Eng., **49**(1–2), pp. 123–140.

[7] Jung, S., and Wen, J. T., 2004, "Nonlinear Model Predictive Control for the Swing-up of a Rotary Inverted Pendulum," ASME J. Dyn. Syst., Meas., Control, **126**(3), pp. 666–673.

[8] Utkin, V. I., 1977, "Variable Structure Systems With Sliding Modes," IEEE Trans. Autom. Control, **22**, pp. 212–222.

[9] Salamci, M. U., Ozgoren, M. K., and Banks, S. P., 2000, "Sliding Mode Control With Optimal Sliding Surfaces for Missile Autopilot Design," J. Guid. Control Dyn., **23**, pp. 719–727.

[10] Tokat, S., Eksin, I., Guzelkaya, M., and Soylemez, M. T., 2003, "Design of a Sliding Mode Controller With a Nonlinear Time-Varying Sliding Surface," Trans. Inst. Meas. Control, **25**, pp. 145–162.

[11] Kim, K. S., and Park, Y., 2004, "Sliding Mode Design via Quadratic Performance Optimization With Pole-Clustering Constraint," SIAM J. Control Optim., **43**, pp. 670–684.

[12] Nikkhah, M., Ashrafiuon, H., and Muske, K., 2006, "Optimal Sliding Control for Underactuated Systems," *Proceedings of the 2006 American Control Conference*, pp. 4688–4693.

[13] Muske, K. R., Ashrafiuon, H., and Nikkhah, M., 2007, "A Predictive and Sliding Mode Cascade Controller," *Proceedings of the 2007 American Control Conference*, pp. 4688–4693.

[14] Bergerman, M., and Xu, Y., 1996, "Robust Joint and Cartesian Control of Underactuated Manipulators," ASME J. Dyn. Syst., Meas., Control, **118**, pp. 557–565.

[15] Lee, K., Coats, S., and Coverstone-Carroll, V., 1997, "Variable Structure Control Applied to Underactuated Robots," Robotica, **15**, pp. 313–318.

[16] Su, C., and Stepanenko, Y., 1999, "Adaptive Variable Structure Set-Point Control of Underactuated Robots," IEEE Trans. Autom. Control, **44**, pp. 2090–2093.

[17] Xu, R., and Ozgüner, U., 2008, "Sliding Mode Control of a Class of Underactuated Systems," Automatica, **44**(1), pp. 233–241.

[18] Olfati-Saber, R., 2002, "Normal Form for Underactuated Mechanical Systems With Symmetry," IEEE Trans. Autom. Control, **47**, pp. 305–308.

[19] Park, M., Chwa, D., and Hong, S., 2006, "Decoupling Control of a Class of Underactuated Mechanical Systems Based on Sliding Mode Control," *Proceedings of the SICE-ICASE International Joint Conference*, pp. 806–810.

[20] Martinez, R., Alvarez, J., and Orlov, Y., 2008, "Hybrid Sliding-Mode-Based Control of Underactuated Systems With Dry Friction," IEEE Trans. Ind. Electr., **55**(11), pp. 3998–4003.

[21] Lee, S. H., Park, J. B., and Choi, Y. H., 2009, "Finite-Time Control of Nonlinear Underactuated Systems Using Terminal Sliding Surface," *Proceedings of the IEEE International Symposium on Industrial Electronics*, pp. 626–631.

[22] Sankaranarayanan, V., and Mahindrakar, A., 2009, "Control of a Class of Underactuated Mechanical Systems Using Sliding Modes," IEEE Trans. Rob., **25**(2), pp. 459–467.

[23] Brockett, R. W., 1983, "Asymptotic Stability and Feedback Linearization," Diff. Geom. Cont. Theory, pp. 181–191.

[24] Riachy, S., Orlov, Y., Floquet, T., Santiesteban, R., and Richard, J.-P., 2008, "Second-Order Sliding Mode Control of Underactuated Mechanical Systems I: Local Stabilization With Application to an Inverted Pendulum," Int. J. Robust Nonlinear Control, **18**(4–5), pp. 529–543.

[25] Santiesteban, R., Floquet, T., Orlov, Y., Riachy, S., and Richard, J.-P., 2008, "Second-Order Sliding Mode Control of Underactuated Mechanical Systems II: Orbital Stabilization of an Inverted Pendulum With Application to Swing Up/Balancing Control," Int. J. Robust Nonlinear Control, **18**(4–5), pp. 544–556.

[26] Ashrafiuon, H., and Erwin, R. S., 2008, "Sliding Mode Control of Underactuated Multibody Systems and Its Application to Shape Change Control," Int. J. Control, **81**, pp. 1849–1858.

[27] Avis, J. M., Nersesov, S. G., Nathan, R., Ashrafiuon, H., and Muske, K. R., 2010, "A Comparison Study of Nonlinear Control Techniques for the RTAC System," Nonlinear Anal.: Real World Appl., **11**(4), pp. 2647–2658.

[28] Garcia-Gabin, W., and Camacho, E., 2003, "Sliding Mode Model Based Predictive Control for Non Minimum Phase Systems," *Proceedings of the European Control Conference*, pp. 957–962.

[29] Perez, M., Jimenez, E., and Camacho, E., 2010, "Design of an Explicit Constrained Predictive Sliding Mode Controller," IET Control Theory Appl., **4**(4), pp. 552–562.

[30] Zhou, J.-S., Liu, Z.-Y., and Pei, R., 2001, "A New Nonlinear Model Predictive Control Scheme for Discrete-Time System Based on Sliding Mode Control," *Proceedings of the American Control Conference*, Vol. 4, pp. 3079–3084.

[31] Slotine, J.-J. E., and Li, W., 1991, *Applied Nonlinear Control*, Prentice-Hall, Englewood Cliffs, NJ.

[32] Khalil, H. K., 2002, *Nonlinear Systems*, 3rd ed., Prentice-Hall, Upper Saddle River, NJ.

[33] Bhat, S. P., and Bernstein, D. S., 2003, "Nontangency-Based Lyapunov Tests for Convergence and Stability in Systems Having a Continuum of Equilibria," SIAM J. Control Opt., **42**(5), pp. 1745–1775.

[34] Spong, M. W., 1997, "Underactuated Mechanical Systems," *Control Problems in Robotics and Automation*, B. Siciliano and K. Valavanis, eds., Springer-Verlag, London.

[35] Nersesov, S. G., Ashrafiuon, H., and Ghorbanian, P., 2010, "On the Stability of Sliding Mode Control for a Class of Underactuated Nonlinear Systems," *Proceedings of the 2010 American Control Conference*, pp. 3446–3551.

[36] Bryson, A. E., and Ho, Y.-C., 1975, *Applied Optimal Control*, Revised ed., Taylor & Francis, Levittown, PA.

[37] Costa, E. F., and do Val, J. B. R., 2009, "Uniform Approximation of Infinite Horizon Control Problems for Nonlinear Systems and Stability of the Approximating Controls," IEEE Trans. Autom. Control, **54**(4), pp. 881–886.

[38] Aosta, J. A., 2010, "Furuta's Pendulum: A Conservative Nonlinear Model for Theory and Practise," Math. Probl. Eng., 2010, Article ID 742894.